High-Precision Determination of g Factors and Masses of $^{20}Ne^{9+}$ and $^{22}Ne^{9+}$

F. Heiße,[1,*] M. Door,[1,†] T. Sailer,[1] P. Filianin,[1] J. Herkenhoff,[1] C. M. König,[1] K. Kromer,[1] D. Lange,[1] J. Morgner,[1] A. Rischka,[1] Ch. Schweiger,[1] B. Tu,[1] Y. N. Novikov,[2,3] S. Eliseev,[1] S. Sturm,[1] and K. Blaum[1]

[1]*Max-Planck-Institut für Kernphysik, Heidelberg, Germany*
[2]*Kurchatov Institute-PNPI, 188300 Gatchina, Russia*
[3]*Saint Petersburg State University, 199034 Saint Petersburg, Russia*

(Received 24 May 2023; revised 11 August 2023; accepted 5 September 2023; published 18 December 2023)

We present the measurements of individual bound electron g factors of $^{20}Ne^{9+}$ and $^{22}Ne^{9+}$ on the relative level of 0.1 parts per billion. The comparison with theory represents the most stringent test of bound-state QED in strong electric fields. A dedicated mass measurement results in $m(^{20}\mathrm{Ne}) = 19.992\,440\,168\,77(9)$ u, which improves the current literature value by a factor of 18, disagrees by 4 standard deviations, and represents the most precisely measured mass value in atomic mass units. Together, these measurements yield an electron mass on the relative level of 0.1 ppb with $m_e = 5.485\,799\,090\,99(59) \times 10^{-4}$ u as well as a factor of seven improved $m(^{22}\mathrm{Ne}) = 21.991\,385\,098\,2(26)$ u.

DOI: 10.1103/PhysRevLett.131.253002

The theory of quantum electrodynamics (QED) successfully describes a broad scope of phenomena ranging from elementary particle physics to atoms and molecules [1–3]. Since QED is a blueprint for all quantum field theories, it is of utmost importance to verify its sophisticated calculation methods as precisely as possible [4,5]. In particular, the deviation between the experimental results and the theoretical prediction for muon $g-2$ [6], muonic deuterium hyperfine splitting [7], as well as the fine structure anomaly in heavy muonic systems [8], currently challenge our understanding of QED. This calls for additional high-precision QED tests. Furthermore, based on such comparisons fundamental constants can be extracted, e.g., the fine structure constant α [4], the Rydberg constant R_∞ [9,10], as well as the electron, proton, deuteron, muon, and charged pion masses [11–17].

The determination of magnetic moments and Lamb shifts of bound leptons allows tests of bound state (BS) QED under extreme conditions, such as strong electric and magnetic fields [18–22]. In this Letter, we present a BS-QED test with highest precision by comparing state-of-the-art bound-electron g-factor calculations of $^{20}Ne^{9+}$ and $^{22}Ne^{9+}$ with corresponding experimental results. The electron g factor is a dimensionless constant relating the electron's magnetic moment to its spin. The energy splitting of the Zeeman levels in a magnetic field B is given by $h\nu_L = h(g/2)(e/2\pi m_e)B$ [23]. Here, ν_L is the Larmor spin precession frequency of an electron, h is the Planck's constant, and (e/m_e) is the electron's charge-to-mass ratio. Additionally, the free-space cyclotron frequency of an ion in the magnetic field can be expressed by $\nu_c = (1/2\pi)(q_{ion}/m_{ion})B$, where (q_{ion}/m_{ion}) is the charge-to-mass ratio of the ion. Combining both equations yields

$$g_{exp} = 2\frac{\nu_L}{\nu_c}\frac{m_e}{m_{ion}}\frac{q_{ion}}{e} = 2\Gamma\frac{m_e}{m_{ion}}\frac{q_{ion}}{e}. \quad (1)$$

In this Letter, the Γ measurement is performed at the ALPHATRAP setup [24], while the mass of $^{20}Ne^{10+}$ is measured at the PENTATRAP experiment [25]. The charge ratio (q_{ion}/e) is a known integer number and the electron mass as well as the mass of $^{22}Ne^{9+}$ are determined by other experiments [11,26].

The mass of $^{20}Ne^{10+}$ is determined by measuring the cyclotron-frequency ratio $\mathcal{R}^{CF} = [\nu_c(^{20}Ne^{10+})/\nu_c(^{12}C^{6+})]$. Given both ν_c measurements are carried out in the same B field, the $^{20}Ne^{10+}$ mass can be expressed by $m(^{20}Ne^{10+}) = (10/6)m(^{12}C^{6+})/\mathcal{R}^{CF}$. The ion masses are linked to $m(^{20}Ne^{9+})$ and the neutral masses via the mass of the missing electrons [27] and binding energies [28], which are known to sufficient precision.

The PENTATRAP and ALPHATRAP experiments are both cryogenic Penning-trap setups located at the Max Planck Institute for Nuclear Physics in Heidelberg. Their trap and detection electronics are cooled to the temperature of liquid helium (4 K). The highly charged ions are produced externally in Heidelberg compact electron beam ion traps (HC-EBITs) [29,30], transferred via room temperature

TABLE I. Trap properties of the ALPHATRAP and PENTATRAP experiments. The magnetic field inhomogeneities are defined via $B(z) = B_0 + B_1 z + B_2 z^2$, where z is the axial position. The different ν_+ for PT and AT are for $^{20}Ne^{9+}$ and $^{22}Ne^{9+}$, respectively.

	ALPHATRAP		PENTATRAP	
	PT	AT	Trap 2	Trap 3
B_0 (T)	≈4	≈3.9	≈7	
B_1 (mT/m)	2.64(3)	$0(1) \times 10^4$	1.41(27)	−1.49(16)
B_2 (mT/m^2)	64(3)	$43.1(1) \times 10^6$	64(5)	22(5)
ν_+ (MHz)	≈28/25	≈27/24	≈54	
ν_z (kHz)	≈651	≈334	≈736	≈502
ν_- (kHz)	≈8	≈2	≈5	≈2
ν_L (GHz)	≈113	≈108	⋯	⋯
T_z (K)	5.7(3)		7(2)	

beamlines to the respective trap setups and cleaned from possible contamination ions via magnetron cleaning [31].

Because of the superposition of the static electric and magnetic field, the cyclotron frequency splits into three individual eigenfrequencies: the axial ν_z, the magnetron ν_-, and the modified cyclotron frequency ν_+, see Table I. Combined, these frequencies can be utilized to calculate the free-space cyclotron frequency $\nu_c = \sqrt{\nu_+^2 + \nu_z^2 + \nu_-^2}$ [32]. Because of the strong hierarchy of the eigenfrequencies, ν_+ has to be determined with highest precision, followed by ν_z and ν_-.

In both experiments the ion's eigenfrequencies are measured nondestructively. The ion's axial oscillations induce fA image currents in high-impedance cryogenic tank circuits [33,34] leading to a measurable voltage signal, see Fig. 1. Interaction with the tank circuit, typically referred to as resistive cooling, causes a temperature of the axial motion near 4 K. Here, the ion effectively shorts the ambient Johnson-Nyquist noise [35,36], leading to the characteristic dip in the spectrum. The axial frequency can be directly measured by fitting the well-known dip line shape to the spectrum. The radial frequencies are measured via radio-frequency (RF) sideband coupling to the axial motion, resulting in a double-dip spectrum to extract the initial parameters for the more precise phase sensitive Ramsey-type measurements [37–39].

The PENTATRAP experiment [25,41,42] is designed for high-precision mass-ratio determinations of ions, see Fig. 1. The measurement scheme, similar to previous measurements at the PENTATRAP experiment [42–45], starts with three single ions of two species ($^{20}Ne^{10+}$, $^{12}C^{6+}$) loaded in alternating order into the three central traps. The traps 2 and 3 are used in parallel for the determination of $\mathcal{R}^{CF}$, while the traps 1 and 4 are exclusively used for storage. At PENTATRAP ν_z is simultaneously determined during the longest phase-evolution time of the Ramsey-type ν_+ measurement [42]. This reduces the effect of electric field jitter compared to sequential measurements and allows for shorter overall measurement times. Daily reloading of the ions, as a result of the limited ion lifetime in PENTATRAP, reduces the impact of potential eigenfrequency shifts on $\mathcal{R}^{CF}$ due to hypothetically unnoticed ion contaminations.

PENTATRAP has an active stabilization system for the helium gas pressure and liquid helium level in the cold bore of the magnet, resulting in a very stable magnetic field. The temporal variation is dominated by a constant relative degradation of about 0.3 (ppb/h). Therefore, it is sufficient to measure only one full set of unwrapping phases for different evolution times at the beginning and merely the phase of the shortest (ϕ^{ref}) and longest evolution time ($\phi^{precision}$) in all subsequent measurement cycles to determine ν_+.

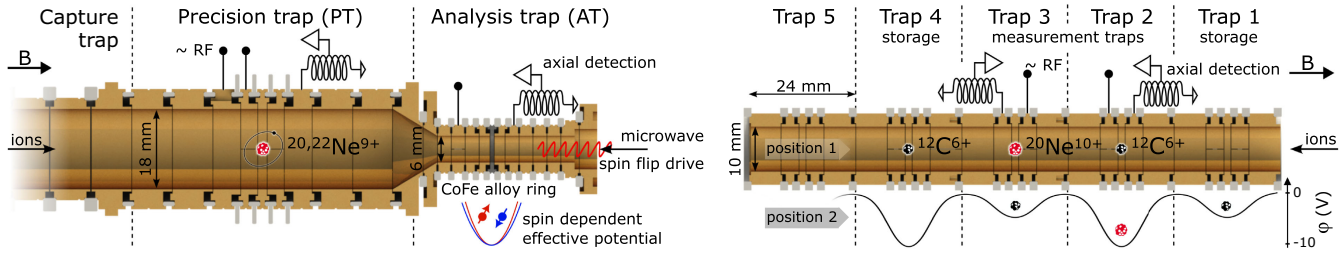

FIG. 1. Sectional views of the cylindrical Penning-trap setups of ALPHATRAP [24] (left) and PENTATRAP [25] (right). Both trap towers are built from gold-plated copper ring electrodes which are isolated by sapphire and quartz rings. The connected superconducting tank circuits, the amplifiers for the axial detection systems, and the RF excitation lines are shown. At the ALPHATRAP experiment, ν_c is measured simultaneously to the irradiation of the microwave drive in the Precision trap. The CoFe alloy central ring electrode in the analysis trap produces a strong magnetic bottle, allowing a nondestructive spin-state detection with close to 100% fidelity. Here, a different spin orientation changes the axial force resulting from the magnetic moment inside the inhomogeneous magnetic field leading to axial frequency jumps of the ion ($^{20,22}Ne^{9+}$ yield jumps of 1.8 Hz and 1.6 Hz, respectively) [40]. At the PENTATRAP setup, both ions' ν_c are measured successively in each measurement trap, resulting in one cyclotron frequency ratio per trap. The ion species are effectively swapped in the measurement traps by adiabatically transporting all ions to the respective neighboring trap and back (position 1 and 2). The different trapping potential depths (ϕ) in the two measurement traps are due to different resonance frequencies of the axial detection circuits.

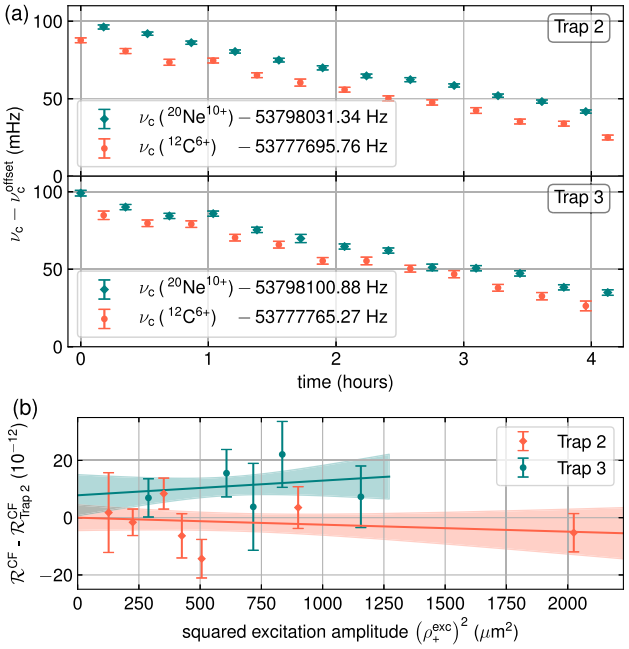

FIG. 2. (a) Exemplary ν_c data from traps 2 and 3. (b) Determined $\mathcal{R}^{CF}$ for different $(\rho_+^{exc})^2$ including the corresponding least-square fits and 1σ confidence bands with $\chi^2_{red} = 1.11$ and 0.65 for traps 2 and 3, respectively. Higher-order shifts $\propto (\rho_+^{exc})^3$ and $(\rho_+^{exc})^4$ are estimated to be negligible. The $\mathcal{R}^{CF}$ of each trap is extracted from the fit at $(\rho_+^{exc})^2 = 0$ μm^2. This extrapolation reduces the relativistic shift and all other shifts that are proportional to $(\rho_+^{exc})^2$.

After the determinations of ten ϕ^{ref} and ten $\phi^{precision}$ the ion positions are swapped by transporting the ions to the adjacent traps and the phase measurements are repeated. Each cycle, including forty phase measurements, ion cooling, and transports, takes about 22 min. An example of measurement data is shown in Fig. 2(a). To accommodate for the slow magnetic field loss of our magnet, each cycle's $\mathcal{R}^{CF}$ is determined using interpolated data of the free cyclotron frequencies of the two ions to a common time in each trap [44].

The statistical shot-to-shot jitter of $\mathcal{R}^{CF}$ (about 7×10^{-11}) originates mainly from the ion's thermally distributed initial radius of the modified cyclotron motion, which averages to approximately 2 μm and takes a slightly different value after each cooling cycle. This distribution persists after the excitation pulse for the Ramsey-type measurement scheme and results in a variation of the relativistic frequency shift on ν_+. These fluctuations lead to a phase jitter that increases linearly with the phase evolution time and thus limit the phase evolution time to 20 s. The excitation radii were varied between $\rho_+^{exc} =$ 15–50 μm to extrapolate $\mathcal{R}^{CF}$ to virtually zero excitation for each trap [31,46], see Fig. 2(b).

All systematic effects are summarized in Table II. The main systematic uncertainties are caused by the dip-fit line shape [47], the nonlinear phase readout effect [44], and by the trapping-potential depth difference to match the two ions' axial frequencies with the detection systems resonance [42].

TABLE II. Relative systematic corrections and their uncertainties on $\mathcal{R}^{CF}$ at PENTATRAP after the extrapolation to zero-excitation amplitude for both traps. All values are given in parts per trillion (10^{-12}). The systematic shifts are assumed to be uncorrelated between the traps.

Effect (parameters)	Trap 2	Trap 3
T_z (B_2, C_3, C_4, C_6)	−0.8(0.3)	−1.7(0.5)
Magnetron frequency	0.0(0.5)	0.0(0.5)
Nonlinear phase readout [44]	0.0(1.0)	0.0(1.9)
Position difference [42]	0.0(1.0)	0.0(0.8)
Dip line shape [47]	0.0(1.0)	0.0(1.8)
Image charge shift [48–50]	19.5(1.0)	19.5(1.0)
Total	18.7(2.1)	17.8(3.0)

Given these effects, the determined $\mathcal{R}^{CF}$ for both traps are

$$\mathcal{R}^{CF}_{trap\,2} = 1.000\,378\,141\,801(5)(2),$$
$$\mathcal{R}^{CF}_{trap\,3} = 1.000\,378\,141\,807(7)(3),$$

with the first and the second bracket showing the statistical and systematic uncertainty, respectively. The weighted mean of the two traps yields $\mathcal{R}^{CF}_{mean} = 1.000\,378\,141\,802(4)$. To determine $m(^{20}Ne)$, we added the masses of the missing electrons and their corresponding binding energies [11,28] with an additional uncertainty of 2×10^{-11} u resulting in

$$m(^{20}Ne) = 19.992\,440\,168\,77(9)\ \text{u}.$$

This represents the most precise mass value ever measured in atomic mass units and deviates by 4σ from the current literature value [26,51]. The achieved precision for an absolute atomic mass demonstrates the capability for order of magnitude improved $m(^{133}Cs)$ and $m(^{87}Rb)$, which is of utmost importance for the determination of α via photon-recoil experiments [52,53].

The g-factor measurements were carried out in the ALPHATRAP setup [24,54,55]. A cryovalve separates the beamline vacuum and the trap vacuum to achieve month-long ion lifetimes.

The setup includes an analysis trap (AT) enabling the detection of the electron's spin-state orientation with respect to the magnetic field via the continuous Stern-Gerlach effect [40,56] as well as a spectroscopic precision trap (PT), distinguished by a harmonic electric and a homogeneous magnetic field, see Fig. 1.

The double-trap measurement sequence is similar to [11,57]. Each measurement cycle begins by placing the respective single neon ion in the AT and determining the

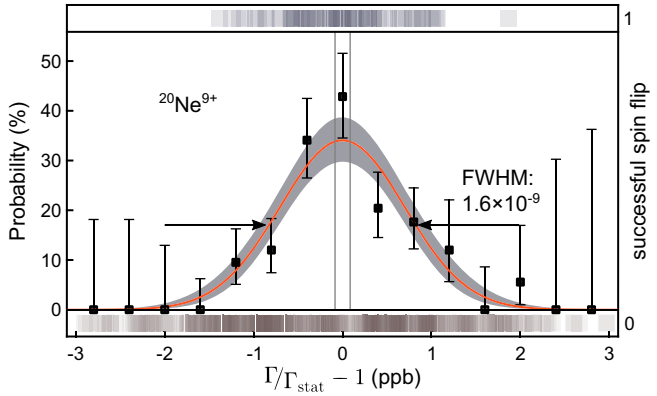

FIG. 3. Γ resonance for $^{20}Ne^{9+}$ containing 425 cycles and fitted via the Maximum-likelihood method with a three-parameter Gaussian line shape (red line), since asymmetric effects shift the resonance center far below the ppt level [32,57,58]. The 1-σ confidence band of the fit is displayed in grey. The black binned data points with binomial error bars are presented to guide the eye. The grey shadows at the top are observed spin flips in the PT for the respective Γ, whereas the ones at the bottom are no spin flips.

electron spin state via microwave irradiation at the corresponding Larmor frequency of the AT. Next, it is transported into the PT to measure ν_z and ν_+ via the dip and double-dip method followed by the phase-sensitive measurement of ν_+ [39]. During the longest phase-evolution time of ν_+ (8 s in this Letter), a microwave (MW) pulse ν_{MW} is simultaneously irradiated around the expected ν_L. Together with ν_c this yields one $\Gamma_i = (\nu_{MW}/\nu_c)$. Finally, the ion is transported back into the AT for the spin-state determination, resulting in a cycle length of 25 min.

For each cycle with a spin-state change in the PT, the corresponding Γ_i is assigned with 1, whereas in the other case with 0. This Boolean information of different probed Γ_i's results in a probability distribution (resonance), see Fig. 3. The resonance width is mainly given by the intrinsic magnetic field fluctuations during the 8 s probe time of Γ.

The main systematic correction of $\Gamma(^{20}Ne^{9+})$ and $\Gamma(^{22}Ne^{9+})$ is due to the special relativity effect caused by the excited cyclotron radii of $\rho_+^{exc} \approx 20$ μm for both isotopes. It amounts to a relative shift of $-5.3(11) \times 10^{-11}$. The image charge shift correction is $-2.5(1) \times 10^{-11}$ [48–50]. Corrections and uncertainties due to magnetic inhomogeneities, electric field anharmonicities, and dip line shapes are on or below the 5×10^{-12} level.

After finishing all measurements, we identified an unexpected systematic shift originating from a technical peculiarity of the cryogenic RF switches during the phase sensitive detection of ν_+. Test measurements set an upper limit of a potential systematic shift of Γ at relative 3.0×10^{-11}, for more details see Ref. [59]. The final results of both $\Gamma(^{20,22}Ne^{9+})$, corrected for systematic effects, are summarized in Table III and are limited by statistics.

TABLE III. The measured Γ's with the ALPHATRAP apparatus for $^{20,22}Ne^{9+}$ are given including their statistic and systematic uncertainties. Measured and theoretical g factors are shown with combined uncertainties. For the g factors determinations the current recommended literature value of m_e [27], the literature value of $m(^{22}Ne)$ [26] and $m(^{20}Ne)$ determined in this Letter are used. The individual BS-QED g-factor contributions are only listed below $g(^{20}Ne^{9+})$ since they are equal for both isotopes. The nuclear size and recoil contribution are listed individually.

	$^{22}Ne^{9+}$	$^{20}Ne^{9+}$
Γ	4450.460 396 87(42)(14)	4045.837 341 56(34)(13)
g_{exp}	1.998 767 262 20(174)	1.998 767 276 99(19)
g_{theo}	1.998 767 263 64(12)	1.998 767 277 11(12)
Dirac (relativistic point nucleus) [60]		1.996 445 170 90
Free-electron QED [27]		0.002 319 304 35
BS 1-loop self energy [61–63]		0.000 002 717 05
BS 1-loop vacuum polarization [64]		−0.000 000 063 22
BS 2-loop [64]		−0.000 000 003 17(12)
BS 3-loop [65]		0.000 000 000 03
Recoil [64]	0.000 000 133 10	0.000 000 146 41
Size [64]	0.000 000 004 60 (1)	0.000 000 004 76 (1)

The comparison of the experimental $g(^{20}Ne^{9+})$ with theory [64] yields the most stringent test of BS-QED in strong electric fields to date at a level of 84 ppm, slightly surpassing the test via $g(^{12}C^{5+})$ and $g(^{28}Si^{13+})$ [11,66–68].

The QED binding corrections to the free-electron g factor are calculated in the α expansion and include one-, two-, and three-loop contributions [23]. The one-loop correction is calculated in all orders of $Z\alpha$, whereas for the two-loop correction the perturbation series expansion has been calculated up to $\mathcal{O}((Z\alpha)^5)$ [69]. The estimated uncertainty from the uncalculated terms of $\mathcal{O}((Z\alpha)^6)$ currently limits all the $1s$ g-factor calculation for elements with $Z \geq 4$ [67,70]. The three-loop correction is currently calculated up to $\mathcal{O}((Z\alpha)^2)$ [65]. The relative theory precision of $g(^{20}Ne^{9+})$ is 6×10^{-11} and comparable with our experimental uncertainty.

In this Letter, the one-loop self-energy corrections are tested at an unprecedented level, verifying the corresponding calculations [62,63]. This is complementary to muonic atom spectroscopy, which is dominated by vacuum polarization corrections [22]. In our Letter, the two-loop contributions are tested at the level of 7%, confirming the $Z\alpha$ expansion for intermediate Z. Additionally, the total nuclear recoil contribution of the g factor is precisely verified. This is complementary to the Δg measurement [64], where the differential nuclear recoil contributions have been confirmed without testing any QED correction calculated within the $Z\alpha$ expansion.

Although the previously measured $g_{exp}(^{28}Si^{13+})$ is more precise compared to $g_{exp}(^{20}Ne^{9+})$, the uncalculated

$\mathcal{O}((Z\alpha)^6)$ contributions of $g_{\mathrm{theo}}(^{28}\mathrm{Si}^{13+})$ limit a more stringent QED test in that case. Tests based on the measured $g(^{12}\mathrm{C}^{5+})$ [11] are possible via an independent m_e determination based on the rovibrational transition energies of HD^+ [12–15,71] combined with the proton's and deuteron's atomic masses [26,72]. The precision of $g_{\mathrm{exp,theo}}(^{12}\mathrm{C}^{5+})$ and $m_e(HD^+)$ is higher compared to $g(^{20}\mathrm{Ne}^{9+})$, but the corresponding BS-QED contributions are reduced as well due to their $Z\alpha$ scaling.

Our value and the other measured high-precision g factors ($^{12}\mathrm{C}^{5+}$, $^{28}\mathrm{Si}^{13+}$, and $^{118}\mathrm{Sn}^{49+}$ [73]) constrain uncalculated higher order contributions and eventually experimentally enhance them in the future [67].

The limits set by $g(^{28}\mathrm{Si}^{13+})$ on the $y_e y_n$ coupling constant present in the Higgs-relaxion mixing scenario [74,75] are confirmed by our measurements. The Δg measurement [64] and these g factors give $[g(^{20}\mathrm{Ne}^{9+}) - g(^{22}\mathrm{Ne}^{9+})] - \Delta g = 1.3(1.7) \times 10^{-9}$ yielding a 1-2-3 test to verify quantum mechanics [76–78].

Additionally, Eq. (1) can be rearranged to express the electron mass via the theoretical value g_{theo}:

$$m_e = \frac{1}{2} g_{\mathrm{theo}} \frac{m_{\mathrm{ion}}}{\Gamma} \frac{e}{q_{\mathrm{ion}}} = 5.485\,799\,090\,99(59) \times 10^{-4}\ \mathrm{u}. \tag{2}$$

Our result is in agreement with the current recommended literature value (0.6σ) and a factor of 3 less precise [27].

Solving Eq. (1) for $m(^{22}\mathrm{Ne}^{9+})$ and correcting for the masses of the missing electrons [27] and the corresponding binding energies [28] yields a factor of seven improved mass uncertainty:

$$m(^{22}\mathrm{Ne}) = 21.991\,385\,098\,2(26)\ \mathrm{u},$$

which is in accordance with the literature value (0.8σ) [26].

In conclusion we determined two experimental g factors of $^{20,22}\mathrm{Ne}^{9+}$ and the atomic mass of $^{20}\mathrm{Ne}$ to highest precision. Together with the corresponding theory this yields the most precise test of BS-QED in strong electric fields. The atomic masses of $^{20,22}\mathrm{Ne}$ are improved by a factor of 18 and 7, respectively.

This work is supported by the Max-Planck-Gesellschaft (MPG) and the International Max-Planck Research Schools IMPRS-PTFS and IMPRS-QD. The project received funding from the European Research Council (ERC) under the European Union's Horizon 2020 research and innovation programme under Grant Agreement No. 832848—FunI and by the DFG (German Research Foundation)—Project-ID 273811115—SFB 1225 ISOQUANT. Furthermore, we acknowledge funding and support by the Max Planck, RIKEN, PTB Center for Time, Constants and Fundamental Symmetries. This work comprises parts of the PhD thesis work of M. D. to be submitted to Heidelberg University, Germany.

F. H., M. D., and T. S. contributed equally to this work.

*fabian.heisse@mpi-hd.mpg.de
†menno.door@mpi-hd.mpg.de

[1] S. Tomonaga, On a relativistically invariant formulation of the quantum theory of wave fields, Prog. Theor. Phys. **1**, 27 (1946).
[2] J. Schwinger, On quantum-electrodynamics and the magnetic moment of the electron, Phys. Rev. **73**, 416 (1948).
[3] R. P. Feynman, Space-time approach to quantum electrodynamics, Phys. Rev. **76**, 769 (1949).
[4] X. Fan, T. G. Myers, B. A. D. Sukra, and G. Gabrielse, Measurement of the electron magnetic moment, Phys. Rev. Lett. **130**, 071801 (2023).
[5] T. Aoyama, T. Kinoshita, and M. Nio, Theory of the anomalous magnetic moment of the electron, Atoms **7** (2019).
[6] B. Abi *et al.* (Muon $g-2$ Collaboration), Measurement of the positive muon anomalous magnetic moment to 0.46 ppm, Phys. Rev. Lett. **126**, 141801 (2021).
[7] M. Kalinowski, K. Pachucki, and V. A. Yerokhin, Nuclear-structure corrections to the hyperfine splitting in muonic deuterium, Phys. Rev. A **98**, 062513 (2018).
[8] I. A. Valuev, G. Colò, X. Roca-Maza, C. H. Keitel, and N. S. Oreshkina, Evidence against nuclear polarization as source of fine-structure anomalies in muonic atoms, Phys. Rev. Lett. **128**, 203001 (2022).
[9] C. G. Parthey, A. Matveev, J. Alnis, B. Bernhardt, A. Beyer, R. Holzwarth, A. Maistrou, R. Pohl, K. Predehl, T. Udem, T. Wilken, N. Kolachevsky, M. Abgrall, D. Rovera, C. Salomon, P. Laurent, and T. W. Hänsch, Improved measurement of the hydrogen 1S–2S transition frequency, Phys. Rev. Lett. **107**, 203001 (2011).
[10] A. Antognini *et al.*, Proton structure from the measurement of 2S-2P transition frequencies of muonic hydrogen, Science **339**, 417 (2013).
[11] S. Sturm, F. Köhler, J. Zatorski, A. Wagner, Z. Harman, G. Werth, W. Quint, C. H. Keitel, and K. Blaum, High-precision measurement of the atomic mass of the electron, Nature (London) **506**, 467 (2014).
[12] S. Alighanbari, G. S. Giri, F. L. Constantin, V. I. Korobov, and S. Schiller, Precise test of quantum electrodynamics and determination of fundamental constants with HD^+ ions, Nature (London) **581**, 152 (2020).
[13] S. Patra, M. Germann, J.-P. Karr, M. Haidar, L. Hilico, V. I. Korobov, F. M. J. Cozijn, K. S. E. Eikema, W. Ubachs, and J. C. J. Koelemeij, Proton-electron mass ratio from laser spectroscopy of HD^+ at the part-per-trillion level, Science **369**, 1238 (2020).
[14] I. V. Kortunov, S. Alighanbari, M. G. Hansen, G. S. Giri, V. I. Korobov, and S. Schiller, Proton–electron mass ratio by high-resolution optical spectroscopy of ion ensembles in the resolved-carrier regime, Nat. Phys. **17**, 569 (2021).
[15] S. Alighanbari, I. V. Kortunov, G. S. Giri, and S. Schiller, Test of charged baryon interaction with high-resolution

vibrational spectroscopy of molecular hydrogen ions, Nat. Phys. **19**, 1263 (2023).

[16] W. Liu, M. G. Boshier, S. Dhawan, O. van Dyck, P. Egan, X. Fei, M. Grosse Perdekamp, V. W. Hughes, M. Janousch, K. Jungmann, D. Kawall, F. G. Mariam, C. Pillai, R. Prigl, G. zu Putlitz, I. Reinhard, W. Schwarz, P. A. Thompson, and K. A. Woodle, High Precision measurements of the ground state hyperfine structure interval of muonium and of the muon magnetic moment, Phys. Rev. Lett. **82**, 711 (1999).

[17] M. Trassinelli, D. Anagnostopoulos, G. Borchert, A. Dax, J.-P. Egger, D. Gotta, M. Hennebach, P. Indelicato, Y.-W. Liu, B. Manil, N. Nelms, L. Simons, and A. Wells, Measurement of the charged pion mass using X-ray spectroscopy of exotic atoms, Phys. Lett. B **759**, 583 (2016).

[18] S. Sturm, A. Wagner, B. Schabinger, J. Zatorski, Z. Harman, W. Quint, G. Werth, C. H. Keitel, and K. Blaum, g Factor of Hydrogenlike $Si13+28$, Phys. Rev. Lett. **107**, 023002 (2011).

[19] A. Gumberidze, T. Stöhlker, D. Banaś, K. Beckert, P. Beller, H. F. Beyer, F. Bosch, S. Hagmann, C. Kozhuharov, D. Liesen, F. Nolden, X. Ma, P. H. Mokler, M. Steck, D. Sierpowski, and S. Tashenov, Quantum electrodynamics in strong electric fields: The ground-state lamb shift in hydrogenlike uranium, Phys. Rev. Lett. **94**, 223001 (2005).

[20] P. Beiersdorfer, H. Chen, D. B. Thorn, and E. Träbert, Measurement of the two-loop lamb shift in lithiumlike $U89^+$, Phys. Rev. Lett. **95**, 233003 (2005).

[21] J. Ullmann *et al.*, High precision hyperfine measurements in Bismuth challenge bound-state strong-field QED, Nat. Commun. **8**, 15484 (2017).

[22] I. Beltrami, B. Aas, W. Beer, G. De Chambrier, P. Goudsmit, T. Ledebur, H. Leisi, W. Ruckstuhl, W. Sapp, G. Strassner, A. Vacchi, U. Kiebele, J.-A. Pinston, and R. Weber, New precision measurements of the muonic $3d_{52}-2p_{32}$ X-ray transition in ^{24}Mg and ^{28}Si: Vacuum polarisation test and search for muon-hadron interactions beyond QED, Nucl. Phys. A **451**, 679 (1986).

[23] T. Beier, The g_j factor of a bound electron and the hyperfine structure splitting in hydrogenlike ions}, Phys. Rep. **339**, 79 (2000).

[24] S. Sturm, I. Arapoglou, A. Egl, M. Höcker, S. Kraemer, T. Sailer, B. Tu, A. Weigel, R. Wolf, J. C. López-Urrutia, and K. Blaum, The ALPHATRAP experiment, Eur. Phys. J. Spec. Top. **227**, 1425 (2019).

[25] J. Repp, C. Böhm, J. R. Crespo López-Urrutia, A. Dörr, S. Eliseev, S. George, M. Goncharov, Y. N. Novikov, C. Roux, S. Sturm, S. Ulmer, and K. Blaum, PENTATRAP: A novel cryogenic multi-Penning-trap experiment for high-precision mass measurements on highly charged ions, Appl. Phys. B **107**, 983 (2012).

[26] W. J. Huang, M. Wang, F. G. Kondev, G. Audi, and S. Naimi, The AME 2020 atomic mass evaluation (I). Evaluation of input data, and adjustment procedures, Chin. Phys. C **45**, 030002 (2021).

[27] E. Tiesinga, P. J. Mohr, D. B. Newell, and B. N. Taylor, CODATA recommended values of the fundamental physical constants: 2018, Rev. Mod. Phys. **93**, 025010 (2021).

[28] A. Kramida, Y. Ralchenko, and J. Reader (the NIST ASD Team), Nist atomic spectra database (version 5.9) (2021), 10.18434/T4W30F.

[29] P. Micke, S. Kühn, L. Buchauer, J. R. Harries, T. M. Bücking, K. Blaum, A. Cieluch, A. Egl, D. Hollain, S. Kraemer, T. Pfeifer, P. O. Schmidt, R. X. Schüssler, C. Schweiger, T. Stöhlker, S. Sturm, R. N. Wolf, S. Bernitt, and J. R. Crespo López-Urrutia, The Heidelberg compact electron beam ion traps, Rev. Sci. Instrum. **89**, 063109 (2018).

[30] C. Schweiger, C. M. König, J. R. Crespo López-Urrutia, M. Door, H. Dorrer, C. E. Düllmann, S. Eliseev, P. Filianin, W. Huang, K. Kromer, P. Micke, M. Müller, D. Renisch, A. Rischka, R. X. Schüssler, and K. Blaum, Production of highly charged ions of rare species by laser-induced desorption inside an electron beam ion trap, Rev. Sci. Instrum. **90**, 123201 (2019).

[31] F. Heiße, S. Rau, F. Köhler-Langes, W. Quint, G. Werth, S. Sturm, and K. Blaum, High-precision mass spectrometer for light ions, Phys. Rev. A **100**, 022518 (2019).

[32] L. S. Brown and G. Gabrielse, Geonium theory: Physics of a single electron or ion in a Penning trap, Rev. Mod. Phys. **58**, 233 (1986).

[33] H. Dehmelt, Radiofrequency Spectroscopy of Stored Ions II: Spectroscopy, Adv. At. Mol. Phys. **5**, 109 (1969).

[34] D. J. Wineland and H. G. Dehmelt, Principles of the stored ion calorimeter, J. Appl. Phys. **46**, 919 (1975).

[35] J. B. Johnson, Thermal agitation of electricity in conductors, Phys. Rev. **32**, 97 (1928).

[36] H. Nyquist, Thermal agitation of electric charge in conductors, Phys. Rev. **32**, 110 (1928).

[37] E. A. Cornell, R. M. Weisskoff, K. R. Boyce, R. W. Flanagan, G. P. Lafyatis, and D. E. Pritchard, Single-ion cyclotron resonance measurement of $M(CO^+)/M(N_2^+)$, Phys. Rev. Lett. **63**, 1674 (1989).

[38] E. A. Cornell, R. M. Weisskoff, K. R. Boyce, and D. E. Pritchard, Mode coupling in a Penning trap: π pulses and a classical avoided crossing, Phys. Rev. A **41**, 312 (1990).

[39] S. Sturm, A. Wagner, B. Schabinger, and K. Blaum, Phase-sensitive cyclotron frequency measurements at ultralow energies, Phys. Rev. Lett. **107**, 143003 (2011).

[40] N. Hermanspahn, H. Häffner, H.-J. Kluge, W. Quint, S. Stahl, J. Verdú, and G. Werth, Observation of the continuous stern-gerlach effect on an electron bound in an atomic ion, Phys. Rev. Lett. **84**, 427 (2000).

[41] C. Roux, C. Böhm, A. Dörr, S. Eliseev, S. George, M. Goncharov, Y. N. Novikov, J. Repp, S. Sturm, S. Ulmer, and K. Blaum, The trap design of PENTATRAP, Appl. Phys. B **107**, 997 (2012).

[42] A. Rischka, H. Cakir, M. Door, P. Filianin, Z. Harman, W. J. Huang, P. Indelicato, C. H. Keitel, C. M. König, K. Kromer, M. Müller, Y. N. Novikov, R. X. Schüssler, C. Schweiger, S. Eliseev, and K. Blaum, Mass-difference measurements on heavy nuclides with an eV/c^2 accuracy in the PENTATRAP spectrometer, Phys. Rev. Lett. **124**, 113001 (2020).

[43] R. X. Schüssler *et al.*, Detection of metastable electronic states by Penning trap mass spectrometry, Nature (London) **581**, 42 (2020).

[44] P. Filianin, C. Lyu, M. Door, K. Blaum, W. J. Huang, M. Haverkort, P. Indelicato, C. H. Keitel, K. Kromer, D. Lange, Y. N. Novikov, A. Rischka, R. X. Schüssler, C. Schweiger, S. Sturm, S. Ulmer, Z. Harman, and S. Eliseev, Direct Q-value determination of the β^- decay of ^{187}Re, Phys. Rev. Lett. **127**, 072502 (2021).

[45] K. Kromer, C. Lyu, M. Door, P. Filianin, Z. Harman, J. Herkenhoff, W. Huang, C. H. Keitel, D. Lange, Y. N. Novikov, C. Schweiger, S. Eliseev, and K. Blaum, High-precision mass measurement of doubly magic ^{208}Pb, Eur. Phys. J. A **58**, 202 (2022).

[46] F. Heiße, F. Köhler-Langes, S. Rau, J. Hou, S. Junck, A. Kracke, A. Mooser, W. Quint, S. Ulmer, G. Werth, K. Blaum, and S. Sturm, High-precision measurement of the proton's atomic mass, Phys. Rev. Lett. **119**, 033001 (2017).

[47] S. Rau, F. Heiße, F. Köhler-Langes, S. Sasidharan, R. Haas, D. Renisch, C. E. Düllmann, W. Quint, S. Sturm, and K. Blaum, Penning trap mass measurements of the deuteron and the HD^+ molecular ion, Nature (London) **585**, 43 (2020).

[48] R. S. Van Dyck, F. L. Moore, D. L. Farnham, and P. B. Schwinberg, Number dependency in the compensated Penning trap, Phys. Rev. A **40**, 6308 (1989).

[49] R. S. Van Dyck, D. B. Pinegar, S. Van Liew, and S. L. Zafonte, The UW-PTMS: Systematic studies, measurement progress, and future improvements, Int. J. Mass Spectrom. **251**, 231 (2006).

[50] M. Schuh, F. Heiße, T. Eronen, J. Ketter, F. Köhler-Langes, S. Rau, T. Segal, W. Quint, S. Sturm, and K. Blaum, Image charge shift in high-precision penning traps, Phys. Rev. A **100**, 023411 (2019).

[51] F. DiFilippo, V. Natarajan, K. R. Boyce, and D. E. Pritchard, Accurate atomic masses for fundamental metrology, Phys. Rev. Lett. **73**, 1481 (1994).

[52] R. H. Parker, C. Yu, W. Zhong, B. Estey, and H. Müller, Measurement of the fine-structure constant as a test of the Standard Model, Science **360**, 191 (2018).

[53] L. Morel, Z. Yao, P. Cladé, and S. Guellati-Khélifa, Determination of the fine-structure constant with an accuracy of 81 parts per trillion, Nature (London) **588**, 61 (2020).

[54] I. Arapoglou, A. Egl, M. Höcker, T. Sailer, B. Tu, A. Weigel, R. Wolf, H. Cakir, V. A. Yerokhin, N. S. Oreshkina, V. A. Agababaev, A. V. Volotka, D. V. Zinenko, D. A. Glazov, Z. Harman, C. H. Keitel, S. Sturm, and K. Blaum, g factor of boronlike argon $^{40}Ar^{13+}$, Phys. Rev. Lett. **122**, 253001 (2019).

[55] A. Egl, I. Arapoglou, M. Höcker, K. König, T. Ratajczyk, T. Sailer, B. Tu, A. Weigel, K. Blaum, W. Nörtershäuser, and S. Sturm, Application of the continuous stern-gerlach effect for laser spectroscopy of the $^{40}Ar^{13+}$ fine structure in a penning trap, Phys. Rev. Lett. **123**, 123001 (2019).

[56] H. Dehmelt, Continuous Stern-Gerlach effect: Principle and idealized apparatus, Proc. Natl. Acad. Sci. U.S.A. **83**, 2291 (1986).

[57] F. Köhler, S. Sturm, A. Kracke, G. Werth, W. Quint, and K. Blaum, The electron mass from g-factor measurements on hydrogen-like carbon $^{12}C^{5+}$, J. Phys. B **48**, 144032 (2015).

[58] J. Verdú, S. Djekić, S. Stahl, T. Valenzuela, M. Vogel, G. Werth, T. Beier, H.-J. Kluge, and W. Quint, Electronic g factor of hydrogenlike oxygen $^{16}O^{7+}$, Phys. Rev. Lett. **92**, 093002 (2004).

[59] T. Sailer, Direct Bound-Electron g-Factor Difference Measurement of Coupled Ions at ALPHATRAP, Ph. D. thesis, Heidelberg University, 2022, 10.11588/heidok.00031317.

[60] G. Breit, The magnetic moment of the electron, Nature (London) **122**, 649 (1928).

[61] V. A. Yerokhin, P. Indelicato, and V. M. Shabaev, Evaluation of the self-energy correction to the g factor of S states in H-like ions, Phys. Rev. A **69**, 052503 (2004).

[62] V. A. Yerokhin and Z. Harman, One-loop electron self-energy for the bound-electron g factor, Phys. Rev. A **95**, 060501(R) (2017).

[63] V. A. Yerokhin, C. H. Keitel, and Z. Harman, Nuclear-size self-energy and vacuum-polarization corrections to the bound-electron g factor, J. Phys. B **46**, 245002 (2013).

[64] T. Sailer, V. Debierre, Z. Harman, F. Heiße, C. König, J. Morgner, B. Tu, A. V. Volotka, C. H. Keitel, K. Blaum, and S. Sturm, Measurement of the bound-electron g-factor difference in coupled ions, Nature (London) **606**, 479 (2022).

[65] H. Grotch, Electron g factor in hydrogenic atoms, Phys. Rev. Lett. **24**, 39 (1970).

[66] S. Sturm, A. Wagner, M. Kretzschmar, W. Quint, G. Werth, and K. Blaum, g-factor measurement of hydrogenlike $^{28}Si^{13+}$ as a challenge to QED calculations, Phys. Rev. A **87**, 030501(R) (2013).

[67] A. Czarnecki, M. Dowling, J. Piclum, and R. Szafron, Two-loop binding corrections to the electron gyromagnetic factor, Phys. Rev. Lett. **120**, 043203 (2018).

[68] J. Zatorski, B. Sikora, S. G. Karshenboim, S. Sturm, F. Köhler-Langes, K. Blaum, C. H. Keitel, and Z. Harman, Extraction of the electron mass from g-factor measurements on light hydrogenlike ions, Phys. Rev. A **96**, 012502 (2017).

[69] A. Czarnecki, J. Piclum, and R. Szafron, Logarithmically enhanced Euler-Heisenberg Lagrangian contribution to the electron gyromagnetic factor, Phys. Rev. A **102**, 050801(R) (2020).

[70] K. Pachucki, A. Czarnecki, U. D. Jentschura, and V. A. Yerokhin, Complete two-loop correction to the bound-electron g factor, Phys. Rev. A **72**, 022108 (2005).

[71] J.-P. Karr and J. C. J. Koelemeij, Extraction of spin-averaged rovibrational transition frequencies in HD^+ for the determination of fundamental constants, Mol. Phys., **121**, e2216081 (2023).

[72] D. J. Fink and E. G. Myers, Deuteron-to-proton mass ratio from simultaneous measurement of the cyclotron frequencies of H_2^+ and D^+, Phys. Rev. Lett. **127**, 243001 (2021).

[73] J. Morgner, B. Tu, C. M. Köenig, S. Sailer, F. Heiße, H. Bekker, B. Sikora, C. Lyu, V. A. Yerokhin, Z. Harman, J. R. Crespo Lopez-Urrutia, C. H. Keitel, S. Sturm, and K. Blaum, Stringent test of QED with hydrogenlike tin, Nature (London) **622**, 53 (2023).

[74] V. Debierre, C. Keitel, and Z. Harman, Fifth-force search with the bound-electron g factor, Phys. Lett. B **807**, 135527 (2020).

[75] V. Debierre, N. S. Oreshkina, I. A. Valuev, Z. Harman, and C. H. Keitel, Testing standard-model extensions with isotope shifts in few-electron ions, Phys. Rev. A **106**, 062801 (2022).

[76] S. Weinberg, Quantum mechanics without state vectors, Phys. Rev. A **90**, 042102 (2014).

[77] S. Weinberg, Lindblad decoherence in atomic clocks, Phys. Rev. A **94**, 042117 (2016).

[78] M. G. Raizen, G. Gilbert, and D. Budker, Proposed test of quantum mechanics with three connected atomic clock transitions, Phys. Rev. A **106**, 032209 (2022).